Chemistry–A European Journal
Research Article
doi.org/10.1002/chem.202104016
Chemistry Europe
European Chemical Societies Publishing
www.chemeurj.org

Directed Synthesis and Chemistry of Unsymmetric Dicationic Diboranes and Their Use in Frustrated Lewis Pair-like Chemistry

Lucas Kistner,[a] Dario Kowatsch,[a] Andreas Marz,[a] Elisabeth Kaifer,[a] and Hans-Jörg Himmel*[a]

Abstract: The chemistry of dicationic diboranes with two B^{II} atoms that are engaged in direct B–B bonding is by enlarge unexplored, although these molecules have intriguing properties due to their combined Lewis acidic and electron-donor properties. Unsymmetric dicationic diboranes are extremely rare, but especially attractive due to their polarized B–B bond. In this work we report the directed synthesis of several stable unsymmetric dicationic diboranes by reaction between the electron-rich ditriflato-diborane $B_2(hpp)_2(OTf)_2$ (hpp = 1,3,4,6,7,8-hexahydro-2*H*-pyrimido[1,2-α]pyrimidinate) and phosphino-pyridines, establishing B–N and B–P bonds with the diborane concomitant with triflate elimination. In the case of 2-((ditertbutylphosphino)methyl)pyridine, the B–N bond is formed instantly, but the B–P bond formation requires (due to steric constraints) several days at ambient conditions for completion, creating an intermediate that could be used for frustrated Lewis pair (FLP)-like chemistry. Here we test its reaction with an aldehyde, and propose a new type of FLP-like chemistry.

Introduction

B^{III} compounds like $B(C_6F_5)_3$ are widely applied as Lewis acids.[1,2] In the last decades, they were especially used in frustrated Lewis pair (FLP) chemistry, in combination with a Lewis base bearing sterically-demanding substituents.[3–11] Due to their increased Lewis acidity, B^{III} cations, usually classified as boronium, borenium or borinium ions in dependence of their coordination number (four, three or two, respectively),[12] are especially attractive for a variety of applications.[13–17] However, their high Lewis acidity could lead to undesired side reactions, for example restricted functional group tolerance and vulnerability to moisture, that limit their use. Intense studies in the last decades even succeeded in the isolation of some B^{III} dications. On the other hand, much less is known about monocationic B^{II} compounds, and only a few dicationic B^{II} molecules have been reported.[18] Molecules with two sp^3-hybridized boron atoms are shown in Figure 1, and examples with two sp^2-hybridized boron atoms in Figure 2. All these compounds are diboranes with a direct B-B bond. The first dicationic diboron compound with sp^3-hybridized B^{II} atoms, $[B_2(hpp)_2(NMe_2H)_2]^{2+}$ with a B–B bond length of 1.746(2) Å in the solid state (see first Lewis structure in Figure 1a), with hpp = 1,3,4,6,7,8-hexahydro-2*H*-pyrimido[1,2-α]pyrimidinate), was synthesized in 2007 by our group.[19] In 2016, Kinjo et al.[20] reported a diboron(II) dication with one phenyl and two formally neutral oxazol-2-ylidene units bound to each boron atom (Figure 1a). With 1.841(8) Å, the B–B bond is significantly longer than in the other known dicationic diboranes. Several other dicationic diboranes were synthesized by replacing the triflato (OTf) substituents in $B_2(hpp)_2(OTf)_2$ by chelating neutral donor ligands [for example, 1,2-bis(tetramethylguanidino)-benzene, Figure 1b, or 2,2′-bipyridine].[21] A tetracationic B^{II} compound was also synthesized, in which two $[B_2(hpp)_2]^{2+}$ units are bound to the tetrakisguanidine 1,4,5,8-tetrakis(tetramethylguanidino)-naphthalene (Figure 1c). Formally, dative bonds could be drawn from the neutral substituents (for example, amine, oxazol-2-ylidene or guanidine in Figure 1) to the boron cation. However, in all these compounds a significant portion of the positive charge is delocalized into the nitrogen donor units (see, for example, the mesomeric structures in Figure 1b).

It was even possible to isolate some B^{II} dications with sp^2-hybridized boron atoms. In Figure 2(a), representative examples from the groups of Dehnicke,[22] Braunschweig[23] and Inoue[24] are shown. Examples for B^{II} dications with a bisguanidine substituent and for a B^{II} tetracation with a bridging tetrakisguanidine substituent from our group are included in Figure 2(b).[25] Moreover, we recently reported the first unsymmetric dicationic diboranes with sp^2-hybridized boron atoms (see Lewis structures in Figure 2c). The first compound in Figure 2(c), with a 1,2-bis(tetramethylguanidino)-benzene donor, is the product of

[a] L. Kistner, D. Kowatsch, A. Marz, Dr. E. Kaifer, Prof. H.-J. Himmel
Anorganisch-Chemisches Institut
Ruprecht-Karls Universität Heidelberg
Im Neuenheimer Feld 270, 69120 Heidelberg (Germany)
E-mail: hans-jorg.himmel@aci.uni-heidelberg.de

Supporting information for this article is available on the WWW under https://doi.org/10.1002/chem.202104016

© 2022 The Authors. Chemistry - A European Journal published by Wiley-VCH GmbH. This is an open access article under the terms of the Creative Commons Attribution Non-Commercial License, which permits use, distribution and reproduction in any medium, provided the original work is properly cited and is not used for commercial purposes.

© 2022 The Authors. Chemistry - A European Journal published by Wiley-VCH GmbH

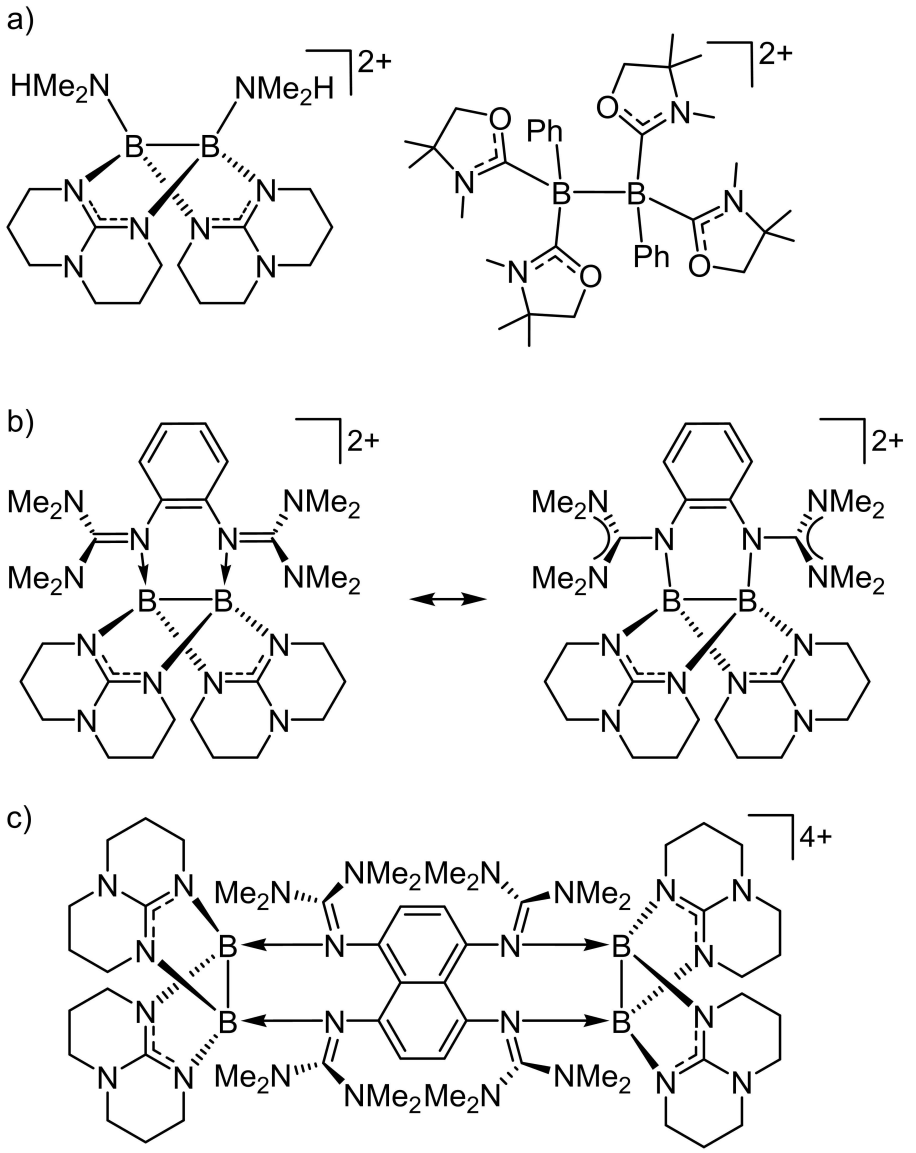

Figure 1. Lewis structures of di- and tetracationic diboranes with sp^3-hybridized boron atoms, with formally neutral amine or oxazol-2-ylidene substituents a) and with bisguanidine b) and tetrakisguanidine c) substituents.

isomerization of the higher-energetic symmetric isomer shown in Figure 2(b) in solution.[25]

In this work, new unsymmetric dicationic diboranes are synthesized by formal addition of a ligand with two different donor sites to the dication $[B_2(hpp)_2]^{2+}$ (see Figure 3), thereby increasing the small number of known unsymmetric dicationic diboranes. The dication $[B_2(hpp)_2]^{2+}$ is generated by triflate elimination from the corresponding ditriflato-diborane $B_2(hpp)_2(OTf)_2$. It could not be isolated, since it immediately dimerizes, in the absence of a donor molecule, to the tetracation $[B_4(hpp)_4]^{4+}$, precipitating together with the counterions from the solution.[26] According to quantum-chemical calculations, $[B_2(hpp)_2]^{2+}$ has a planar B_2N_4 core.[19] Figure 3 displays the Lewis structures of the new unsymmetric dicationic diboranes synthesized in this work starting with the ditriflato-diborane $B_2(hpp)_2(OTf)_2$ and a phosphino-pyridine base. It will be shown that all these dications are stable compounds at ambient conditions. Interestingly, the reaction leading to **5** is much slower than all other reactions; the intermediate $\mathbf{5_{int}}$ (see Lewis structure in Figure 3) is formed immediately, but the ring closing step to give **5** is opposed by a barrier due to steric constraints. We will show that the intermediate $\mathbf{5_{int}}$ could be used in a new type of frustrated Lewis pair (FLP)-like chemistry, using for the first time dicationic diborane Lewis acids.[27] The rapid formation of the B–N bond places the Lewis base close to the Lewis acidic boron atom. Frustration is caused by steric constraints in combination with a triflate elimination equilibrium.

© 2022 The Authors. Chemistry - A European Journal published by Wiley-VCH GmbH

Research Article
doi.org/10.1002/chem.202104016

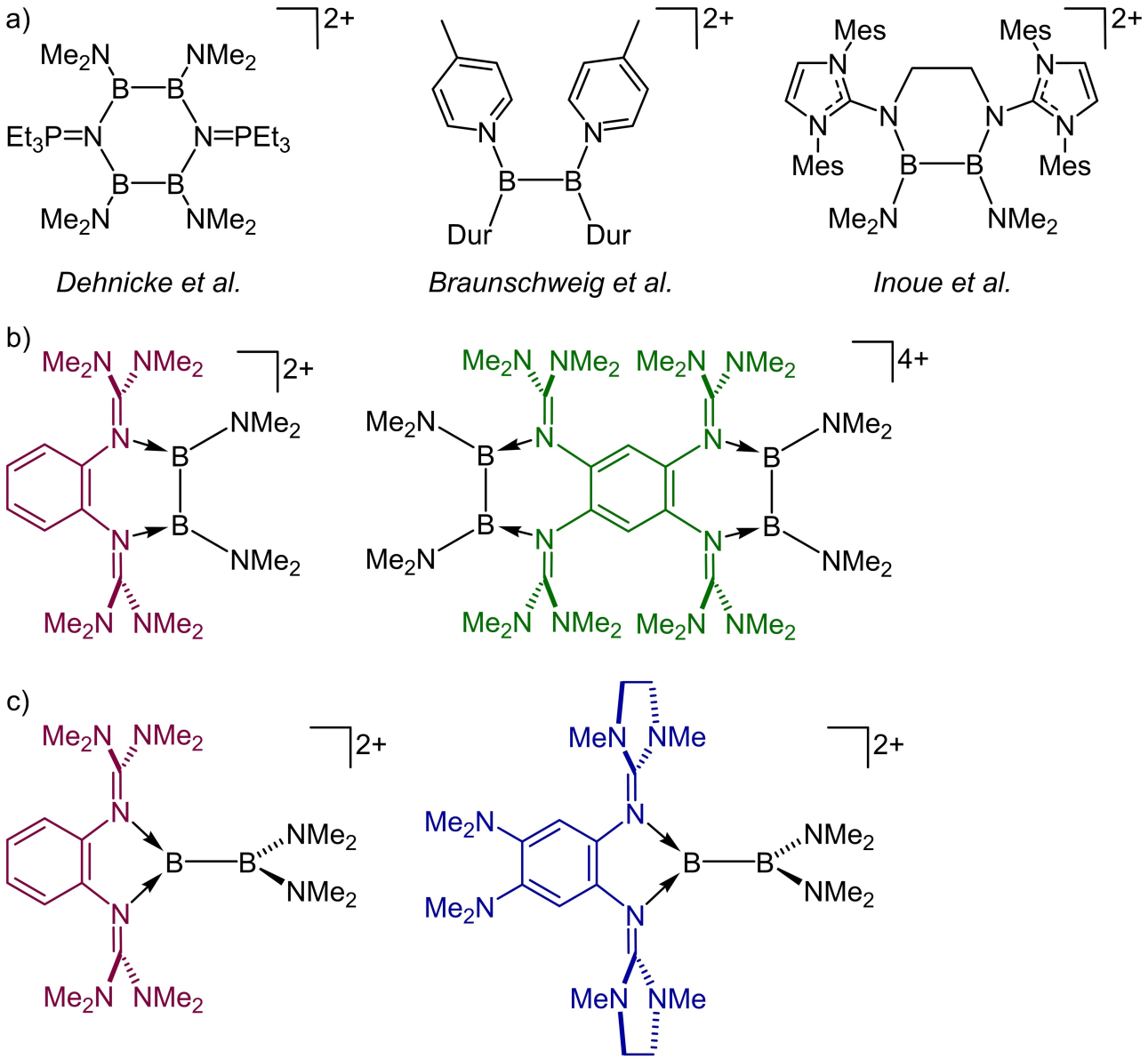

Figure 2. Lewis structures of di- and tetracationic diboranes with sp^2-hybridized boron atoms.

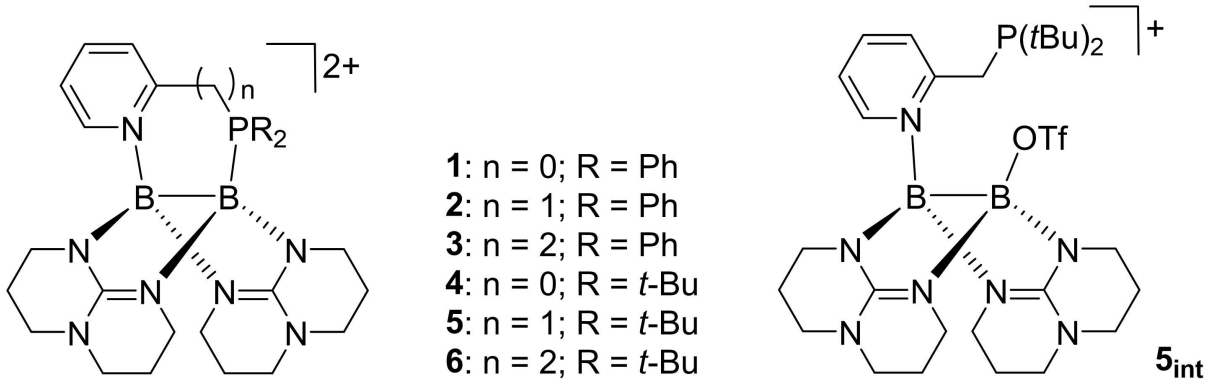

Figure 3. Lewis structures of the five new unsymmetric dicationic diboranes **1**–**5** synthesized in this work, the hypothetical diborane **6**, and the intermediate $\mathbf{5}_{int}$.

© 2022 The Authors. Chemistry - A European Journal published by Wiley-VCH GmbH

Results and Discussion

Synthesis

Reaction of the ditriflato-diborane $B_2(hpp)_2(OTf)_2$ with one of the three applied diphenylphosphino-pyridines sketched in Scheme 1 yielded the dicationic diboranes **1**–**3** in acceptable-good isolated yields (82% for **1**, 54% for **2**, and 49% for **3**, Scheme 1). Both triflates are rapidly eliminated from the ditriflato-diborane reagent. The reactions required only 30 min–2 h for completion. Also, the new dicationic diborane **4**, was synthesized in only 3 h reaction time at room temperature in a yield of 57% from the reaction of $B_2(hpp)_2(OTf)_2$ with 2-(di-*tert*-butylphosphino)pyridine. By contrast, reaction of the ditriflato-diborane $B_2(hpp)_2(OTf)_2$ with 2-((di-*tert*-butyl-phosphino)methyl)pyridine ($pyCH_2PtBu_2$) to give **5** was much slower; 3 d were required for completion. Eventually, pure **5** was isolated in a yield of 80%. We abstained from the synthesis of the dicationic diborane **6**; the synthesis of the corresponding pyridylphosphine ligand by standard procedures turned out to be difficult, and the analysis detailed below indicates that it should exhibit no special properties other than those of compounds **1**–**5**.

Further NMR experiments showed that the reaction to give **5** proceeds in two clearly distinguishable steps. The first step, elimination of the first triflate and formation of a B–N bond with the pyridine N atom to give intermediate $\mathbf{5}_{int}$ (Lewis structure in Figure 4a) occurs instantly upon mixing the two reagents together. In a second, much slower step, the B–P bond is established and the second triflate eliminated to give **5** (Figure 4a). By contrast, no such intermediate, in which only the pyridine N atom is bound directly to the diboron unit, could be detected for compounds **1**–**4**; substitution of the second triflate by the phosphine is too fast to be followed by NMR spectroscopy. On the other hand, the reaction progress for $\mathbf{5}_{int} \rightarrow \mathbf{5}$ can easily be followed by ^{1}H, ^{19}F and ^{31}P NMR spectroscopy. The first ^{19}F NMR spectrum, recorded immediately after mixing the two reactants together (Figure 4a), showed a signal at $\delta = -78.78$ ppm due to free triflate and another signal at $\delta = -77.70$ ppm due to $\mathbf{5}_{int}$ in a ratio close to 1:1. Within 3 d, the signal of $\mathbf{5}_{int}$ vanished and the signal of free triflate gained in intensity, indicating conversion into **5**. In the ^{31}P NMR

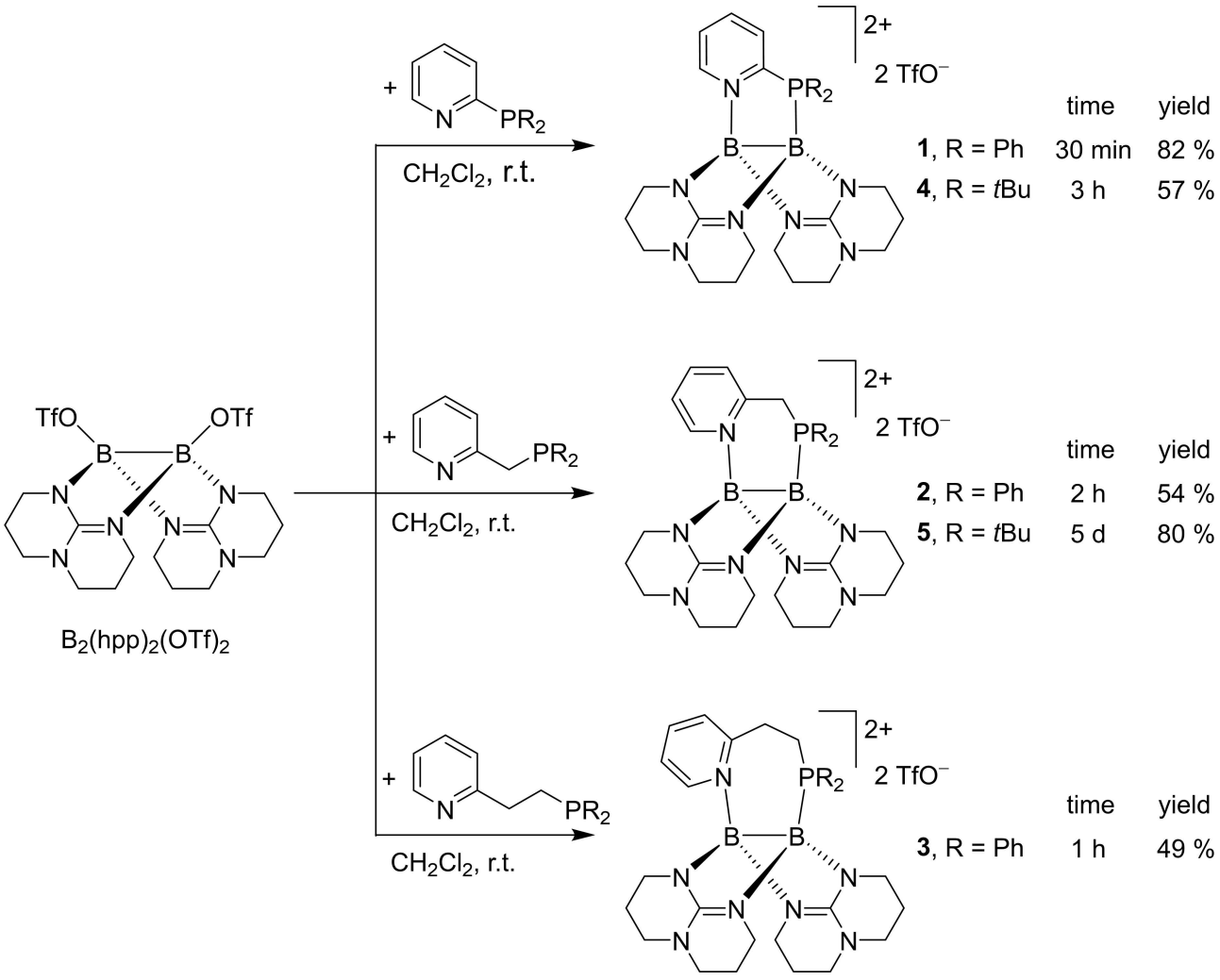

Scheme 1. Reaction of the ditriflato-diborane with different phosphino-pyridine bases.

© 2022 The Authors. Chemistry - A European Journal published by Wiley-VCH GmbH

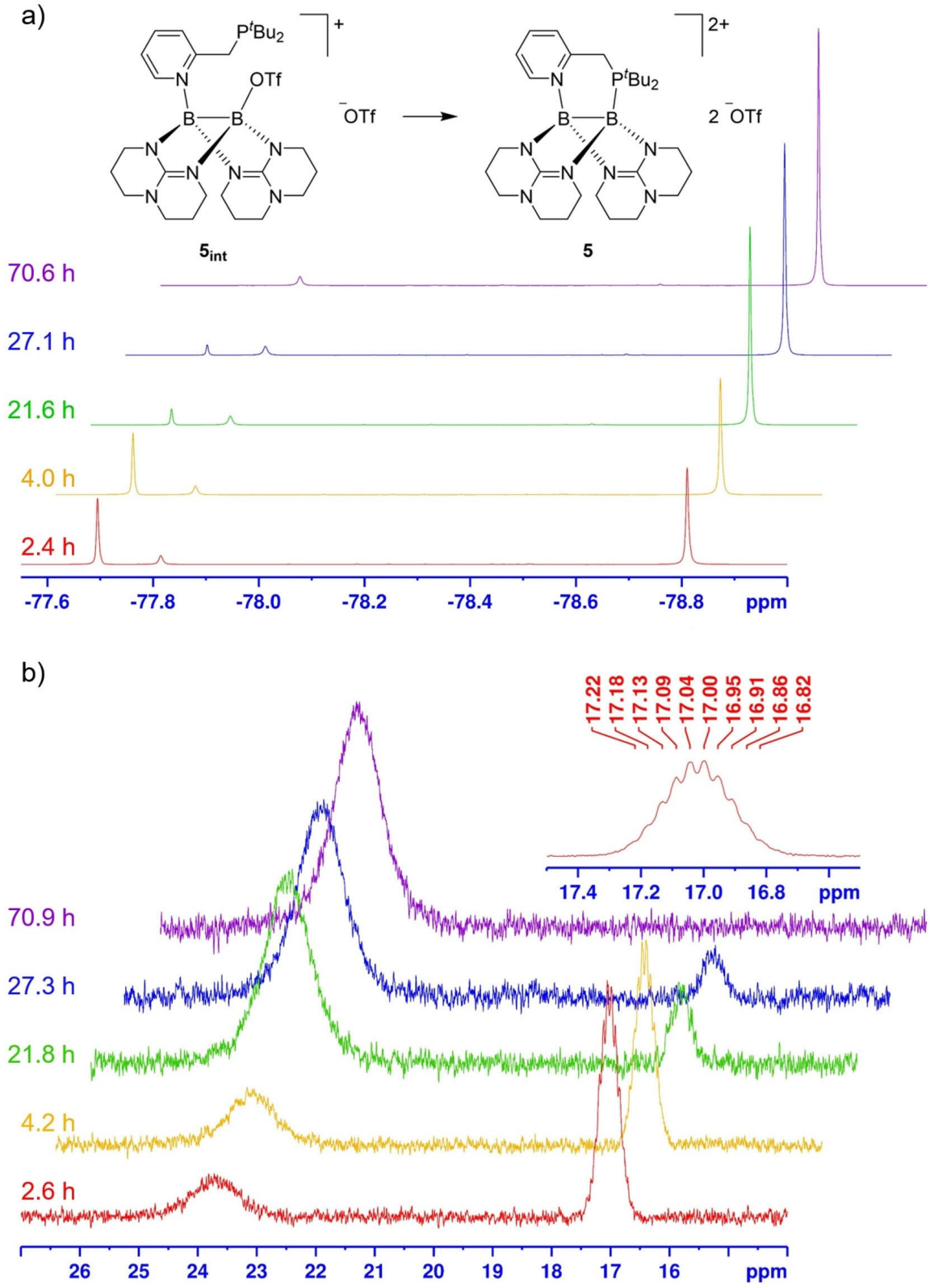

Figure 4. a) ^{19}F NMR spectra (376.27 MHz, CD_2Cl_2) recorded for the conversion of $\mathbf{5}_{int}$(OTf) (signals at $\delta = -77.70$ and -78.78 ppm) to $\mathbf{5}(OTf)_2$ (signal at $\delta = -78.78$) after various reaction times. All intensities are normalized to the slight excess of ditriflato-diborane in the reaction mixture giving a signal at $\delta = -77.81$ ppm. b) ^{31}P NMR spectra (161.88 MHz, CD_2Cl_2) for the conversion of $\mathbf{5}_{int}$ (signal at $\delta = 17.05$ ppm) to **5** (signal at $\delta = 23.62$ ppm), recorded after various reaction times.

© 2022 The Authors. Chemistry - A European Journal published by Wiley-VCH GmbH

spectrum (Figure 4b) recorded immediately after reaction initiation, one major signal at $\delta = 17.05$ ppm due to the intermediate $\mathbf{5}_{int}$ appeared. For comparison, the signal of free $pyCH_2PtBu_2$ shows at $\delta = 36.27$ ppm. The presence of a multiplet signal arising from ^{31}P–^{1}H coupling (see zoom in the inlet of Figure 4b) excludes a direct bonding to a boron nucleus whose quadrupole spin would broaden the ^{31}P NMR signal, thereby prohibiting the observation of such a fine structure. Here, too, the signal from $\mathbf{5}_{int}$ disappeared within 3 d; simultaneously, the broad signal at $\delta = 23.62$ ppm due to **5** grew in intensity. The NMR spectra indicated that a portion of $pyCH_2PtBu_2$ binds instantly with both the pyridine N atom and the P atom to the diboron unit, resulting in immediate formation of ca. 10% of **5** according to the ^{1}H NMR data. To the largest part (ca. 90%) reaction leads first to intermediate $\mathbf{5}_{int}$, that is slowly (within 3 d) converted to **5**, allowing intervention in this process (see below). The conversion of $\mathbf{5}_{int}$ to **5** even takes place if THF or CH_3CN is added to the solution, indicating that these donor solvents do not prohibit reaction.

The evolution of the ^{19}F NMR signal intensities due to $\mathbf{5}_{int}$ and **5** with time allows to estimate the reaction rate (see Supporting Information, Figure S20). The collected data is in line with a first-order rate law with a rate constant $k = 4.94 \pm 0.02$ min^{-1} and a reaction half-life $t_{1/2} = 8.45 \pm 0.03$ h; hence more than 99.9% completion should be achieved after 10 $t_{1/2} = 84.5 \pm 0.3$ h. The reaction was generally run for 5 d to ensure quantitative conversion of $\mathbf{5}_{int}$. Furthermore, the kinetic data confirmed the observation from ^{1}H NMR spectroscopy that some **5** (12% according to the kinetic data from ^{19}F NMR spectroscopy) is instantly formed.

Intriguingly, the ring-closing step from the initially-formed intermediate $\mathbf{5}_{int}$ to the end-product **5** is slow only for reaction with $pyCH_2PtBu_2$. Here, the ^{1}H NMR spectra recorded for $\mathbf{5}_{int}$ proved to be informative. The intermediate gives rise to two doublets at $\delta = 1.18$ ppm ($^{3}J_{HP} = 11.2$ Hz) and 1.15 ppm ($^{3}J_{HP} = 11.8$ Hz) in the ^{1}H NMR spectra at room temperature, with an intensity ratio close to 1:1 (Figure 5, blue curve). These doublets originate from the *tert*-butyl groups and their coupling to the P nucleus. On the other hand, the *tert*-butyl groups of free $pyCH_2PtBu_2$ only give rise to one doublet (Figure 5, red curve). Hence, the equivalence of the *tert*-butyl groups is removed in $\mathbf{5}_{int}$. According to quantum-chemical calculations (B3LYP + D3/def2-TZVP, see Supporting Information), the pyridine ring in $\mathbf{5}_{int}$ is twisted with respect to the B–B bond (leading to a dihedral angle B–B–N–C of 54.9°) and the phosphine residue points away from the B–B axis. Hence, a rotation about the pyridine-methylene bond, positioning the phosphorous atom close to the boron center, is necessary to establish the B–P bond. Apparently, a high barrier evoked by the sterically-demanding *tert*-butyl groups opposes such a rotation. By contrast, the sterically less-demanding phenyl groups in $pyCH_2PPh_2$ allow fast formation of **2**. Also, the formation of **4** does not require such pre-positioning due to the lack of an alkyl spacer in $pyPtBu_2$. Hence, only for the reaction with $pyCH_2PtBu_2$, the intermediate ($\mathbf{5}_{int}$) exhibits a high life-time. The steric constrains imposed by the *tert*-butyl groups and the methylene linker, in combination with the triflate elimination equilibrium, lead to a remarkably slow ring closure reaction rate from $\mathbf{5}_{int}$ to **5**, allowing the use of $\mathbf{5}_{int}$ in FLP-like chemistry (see discussion below).

Crystal structures

The triflate salts of all dicationic diboron compounds **1**–**5** are stable at room temperature and could be stored for longer

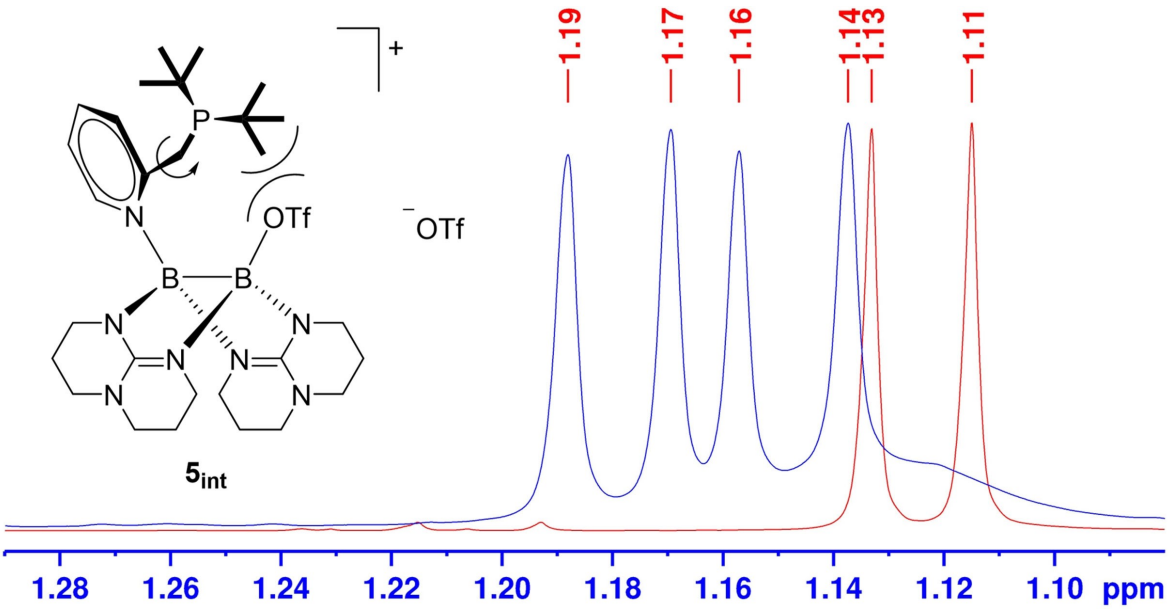

Figure 5. ^{1}H NMR spectrum (600.18 MHz, CD_2Cl_2) of free $pyCH_2PtBu_2$ (red) and $\mathbf{5}_{int}$ (blue) showing the signals due to the *tert*-butyl groups, recorded for a mixture between $pyCH_2PtBu_2$ and $B_2(hpp)_2(OTf)_2$ (after 2 h reaction time).

© 2022 The Authors. Chemistry - A European Journal published by Wiley-VCH GmbH

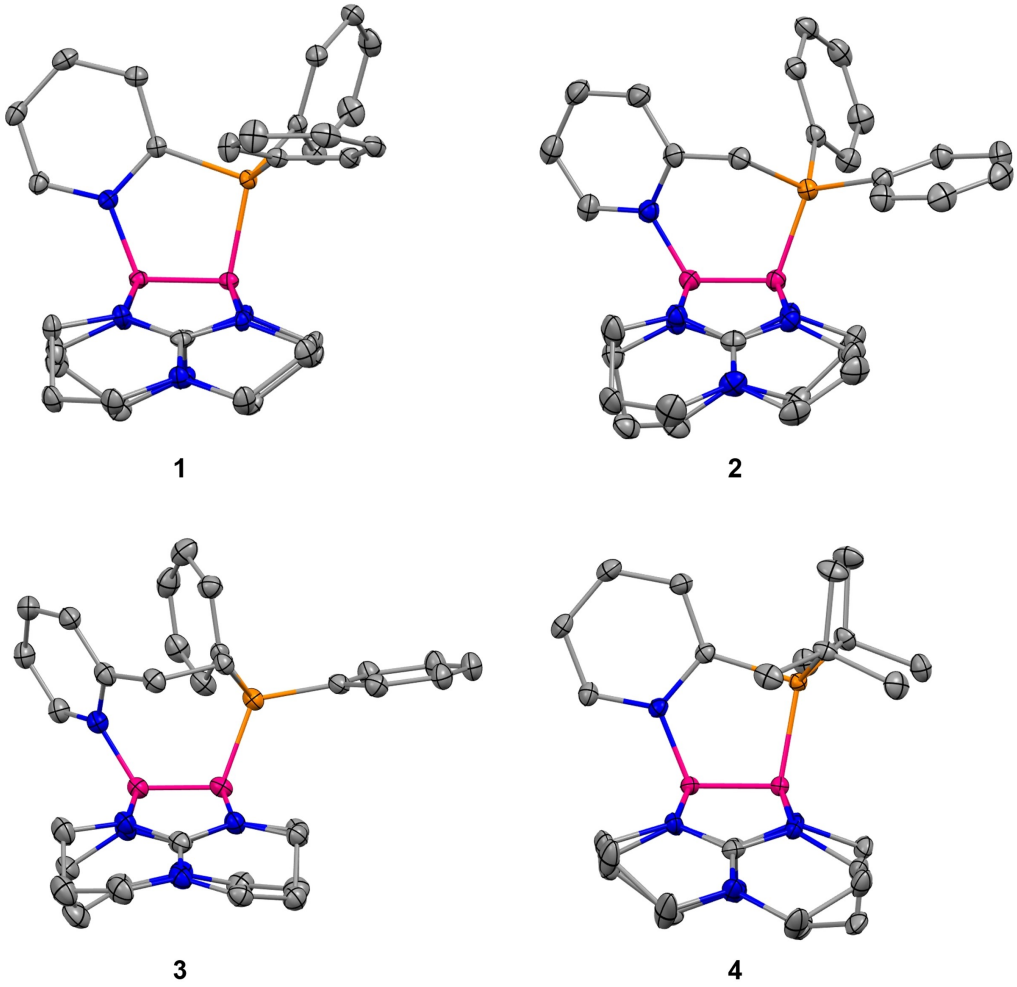

Figure 6. Illustration of the solid-state structures of dications **1**–**4** in the triflate salts. Hydrogen atoms and counterions omitted. Displacement ellipsoids drawn at the 50% probability level. Color code: C grey, B pink, N blue, P orange.

periods without signs of decomposition, even in protic and nucleophilic solvents such as ethanol. Crystals of **1** and **4** suitable for SCXRD were grown by layering a solution of the triflate salts in CH_2Cl_2 with *n*-pentane. Crystals of **2** were obtained by layering an ethanol solution with diethylether, and crystals of **3** by layering a CH_2Cl_2 solution with diethylether. Figure 6 displays the solid-state structures of the new unsymmetric diboron dications with five-membered B_2NCP rings (compounds **1** and **4**), six-membered B_2NC_2P ring (compound **2**) and seven-membered B_2NC_3P ring (compound **3**); Table 1 includes selected structure parameters.[28] With increasing ring size, the dihedral angle B–B–N–C (N and C atoms from the pyridine ring) increases. Compounds **1** and **4** exhibit longer B–P bonds, shorter B-B bonds, and smaller B–B–N and B–B–P angles than **2** and **3**, due to steric constraints imposed by the inflexibility of the phosphino-pyridine.

Table 1. Structure parameters (bond lengths in Å, bond angles in °) for the four new unsymmetric dicationic diboranes **1**–**4** in the solid state.[28]

parameter	**1**[a]		**2**	**3**	**4**
B–B	1.698(3)	1.701(3)	1.726(4)	1.734(6)	1.705(3)
$B–N_{py}$	1.608(2)	1.608(3)	1.606(4)	1.611(5)	1.595(4)
B–P	1.963(2)	1.964(2)	1.949(3)	1.953(4)	2.009(3)
$B–N_{gua}$	1.507(3)	1.513(3)	1.517(4)	1.529(5)	1.527(3)
	1.527(3)	1.523(5)	1.537(4)	1.532(3)	1.527(3)
	1.515(3)	1.521(3)	1.545(4)	1.540(6)	1.524(3)
	1.533(3)	1.525(3)	1.534(4)	1.532(5)	1.521(3)
$B–B–N_{py}$	112.2(1)	112.1(2)	120.8(2)	121.0(3)	112.2(2)
B–B–P	100.1(1)	99.8(1)	108.8(2)	110.5(3)	99.8(1)
B–P–C	97.16(9)	98.12(9)	99.5(1)	106.2(2)	97.0(1)
B–B–N–C	6.2(1)	5.7(1)	29.6(2)	57.5(5)	2.2(3)

[a] Two different molecules in the unit cell.

Electronic properties

In Table 2, the ^{11}B and ^{31}P NMR shifts for compounds **1**–**5** are collected. As expected, two signals show in the ^{11}B NMR spectra. The signals with a positive chemical shift value are assigned to the B atoms attached to the pyridine N atoms, and the other

© 2022 The Authors. Chemistry - A European Journal published by Wiley-VCH GmbH

Table 2. Experimental (in CD_2Cl_2 solution) and calculated (BP86 + D3/def2-SVP) ^{11}B and ^{31}P NMR chemical shifts (in ppm) for compounds **1**–**5**. For comparison, the ^{31}P NMR shifts for the free phosphino-pyridine [denoted P(substrate)] are also included.

	1	**2**	**3**	**4**	**5**
B(N)	9.99	4.08	4.79	9.40	3.62
B(P)	−4.32	−6.14	−6.59	−4.16	−4.38
P	16.84	−4.41	−7.93	47.83	23.67
P(substrate)	−4.01	−11.22	−15.69	39.05	36.27
B(N) calc.	8.93	2.30	4.55	7.87	1.36
B(P) calc.	−3.78	−6.85	−7.02	−4.49	−4.20

Table 4. Gibbs free energy changes (ΔG^0 in kJ mol^{-1} at 298 K, 1 bar) for B–P bond cleavage of **1**–**6** to give $\mathbf{1}_{iso}$–$\mathbf{6}_{iso}$ and hydrogenation of $\mathbf{1}_{iso}$–$\mathbf{6}_{iso}$ (reactions in Scheme 2), calculated with B3LYP + D3/def2-TZVP.

Compound	B–P bond cleavage	Hydrogenation
1	91	1
2	120	−32
3	132	−47
4	103	−22
5	138	−78
6	125	−98

signals, with a negative chemical shift value, to the B atoms attached to the P atoms. This assignment is supported by the results of quantum-chemical calculations (BP86 + D3/def2-SVP, see Table 2). The difference of the ^{11}B NMR chemical shift between the two boron atoms in the unsymmetric dications is a valuable indicator for their different properties. Here, the difference is largest for compounds **1** and **4** [$\Delta\delta(^{11}B) = 14.31$ and 13.56 ppm, respectively] with the phosphino group directly attached to the pyridine ring. In these two compounds, the B–B–N and B–B–P angles are significantly smaller than in compounds **2** and **3**. For compounds **1**–**3** with phenyl groups, the ^{31}P NMR signal is shifted to higher field with respect to the corresponding free phosphino-pyridine (Table 2). For compound **1**, the difference of the ^{31}P NMR shift between the free phosphino-pyridine ($pyPPh_2$) and the dicationic diborane is maximal [$\Delta\delta(^{31}P) = 20.85$ ppm]. In the case of compounds **4** and **5** with *tert*-butyl groups, the ^{31}P NMR signals are shifted in opposite directions. For **4**, the signal shifts to higher field, but for **5** it shifts to lower field with respect to the corresponding free phosphino-pyridines.

Some results of an NBO analysis (from B3LYP + D3/def2-TZVP calculations) for the new unsymmetric dicationic diboranes are included in Table 3. In the case of the closed-ring structures **1**–**6**, the B atom attached to the pyridine N atom [denoted B(N)] carries a high positive formal charge, while the B atom attached to P [denoted B(P)] carries a smaller positive formal charge. The difference between the formal charges on B(N) and B(P) is largest for compounds 2 and 3. The phosphorus atom carries a particularly high formal charge (with a maximum of 1.383 in 2), whereas the charge at the nitrogen atom is slightly less negative than in the corresponding free phosphino-pyridines [N(substrate)].

FLP-like chemistry – part a) theoretical studies

Prior to experiments, we carried out some quantum-chemical calculations to obtain information about the Lewis acidity and possible FLP-like chemistry of the new dicationic diboranes. In these calculations, we applied the B3LYP + D3 method in combination with the def2-TZVP basis set. We used this combination previously for calculations on diboranes with bridging guanidinate substituents,[29] and the general agreement between calculated and experimental results was satisfying. First, the Gibbs free energy changes for B–P bond cleavage, converting compounds **1**–**6** into their isomers $\mathbf{1}_{iso}$–$\mathbf{6}_{iso}$ with a Lewis acidic B atom and a Lewis basic P atom, were inspected (see Scheme 2 and Table 4). They are relatively low, being in the range from 91 kJ mol^{-1} (**1**→$\mathbf{1}_{iso}$) to 138 kJ mol^{-1} (**5**→$\mathbf{5}_{iso}$).

Furthermore, we calculated the thermodynamics and product structures for the reactions of the new diboron dications with dihydrogen. The Gibbs free energy change for hydrogenation according to Scheme 2 varies significantly (Table 4) from $\Delta G = -98$ kJ mol^{-1} and -78 kJ mol^{-1} for compounds $\mathbf{6}_{iso}$ and $\mathbf{5}_{iso}$, respectively, and a maximum of $+1$ kJ mol^{-1} for $\mathbf{1}_{iso}$.

To probe the Lewis acidity of the tri-coordinate boron atom generated after B–P bond cleavage, we calculated the fluoride ion affinity (FIA) for compounds $\mathbf{1}_{iso}$–$\mathbf{6}_{iso}$, in which the B–P bond is already cleaved, relative to that of the dication $[B_2(hpp)_2]^{2+}$ (Scheme 3 and Table 5). It should be noted that steric repulsion between the pyridylphosphino and the fluorido substituents reduces the significance of such calculations. The FIA values for the isolated molecules ($\varepsilon_r = 1$) are smaller than that of $[B_2(hpp)_2]^{2+}$. On the other hand, the inclusion of the solvent effect ($\varepsilon_r = 8.93$ for CH_2Cl_2) turns the FIA values of $\mathbf{1}_{iso}$–$\mathbf{6}_{iso}$ to larger values than for $[B_2(hpp)_2]^{2+}$, except for $\mathbf{4}_{iso}$. Obviously, the solvent effect is particularly large for the small dication

Table 3. Results of a natural bond orbital (NBO) analysis (from B3LYP/def2-TZVP calculations). Formal charges (in e) for compounds **1**–**6** focusing on the central N–B–B–P unit.

Compound	P	N	B(P)	B(N)	P(substrate)[b]	N(substrate)[b]
1	1.327	−0.395	0.113	0.552	0.787	−0.428
2	1.383	−0.413	0.081	0.586	0.831	−0.424
3	1.349	−0.425	0.091	0.614	0.801	−0.437
4	1.293	−0.405	0.169	0.538	0.800	−0.431
5	1.356	−0.423	0.141	0.578	0.816	−0.425
$\mathbf{5}_{iso}$ [a]	0.794	−0.421	0.794	0.454	0.816	−0.425
6	1.296	−0.434	0.208	0.590	0.781	−0.433

[a] See Lewis structure in Scheme 2 and discussion in the next section. [b] Values for the free phosphino-pyridines.

© 2022 The Authors. Chemistry - A European Journal published by Wiley-VCH GmbH

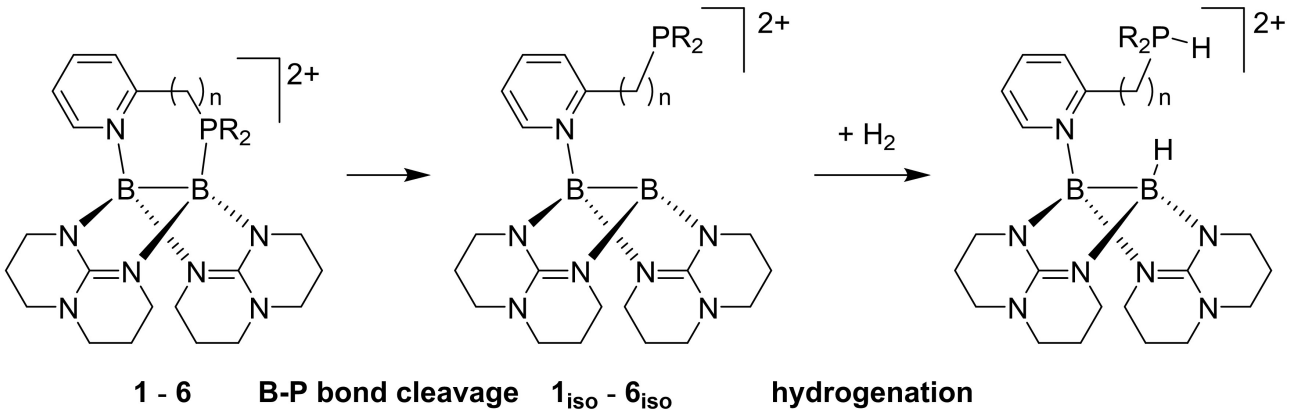

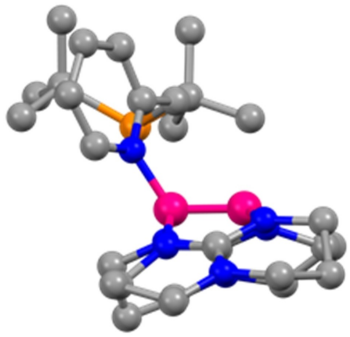

$\mathbf{5_{iso}}$

Scheme 2. Test reactions studied in quantum-chemical calculations (B3LYP + D3/def2-TZVP) to obtain information about the possible FLP-like reactivity of the dicationic diboranes. The illustration of the structure (C grey, B pink, N blue, P orange, H atoms omitted) calculated for $\mathbf{5_{iso}}$ highlights the non-planarity at the tri-coordinate boron atom (see discussion).

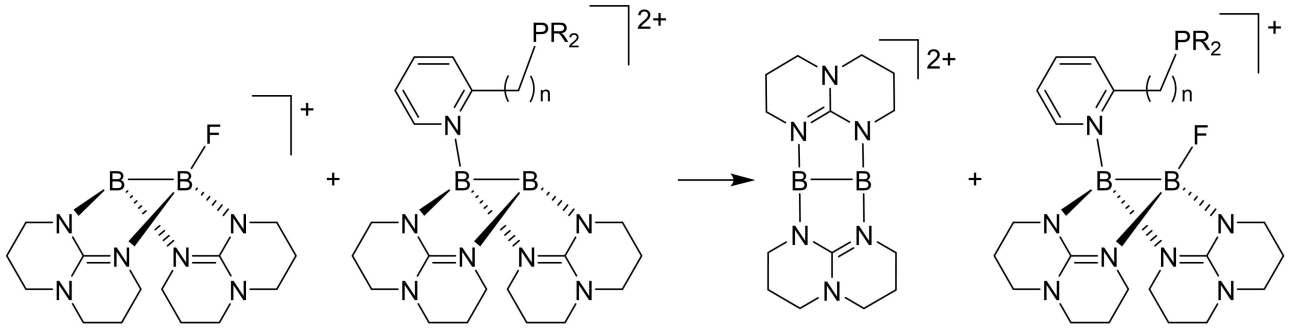

Scheme 3. Test reaction to evaluate the FIA of compounds $\mathbf{1_{iso}}$–$\mathbf{6_{iso}}$ compared to $[B_2(hpp)_2]^{2+}$.

$[B_2(hpp)_2]^{2+}$. Although of limited use due to the differences in charge, we also included the FIA values relative to that of the trimethylsilyl cation (TMS^+). For the isolated compounds ($\varepsilon_r = 1$, gas-phase), the FIA values of the dicationic diboranes are larger than that of TMS^+ for $\mathbf{2_{iso}}$, $\mathbf{3_{iso}}$, $\mathbf{5_{iso}}$ and $\mathbf{6_{iso}}$, but all values are smaller than that of TMS^+ upon inclusion of the solvent effect with COSMO ($\varepsilon_r = 8.93$ for CH_2Cl_2). Obviously, the solvation energy is larger for the dicationic diboranes $\mathbf{1_{iso}}$–$\mathbf{6_{iso}}$ than for the monocationic TMS^+. One could see that the introduction of a methylene (CH_2) spacer between pyridyl and phosphorus increases the FIA (higher FIA of $\mathbf{2_{iso}}$ in comparison to $\mathbf{1_{iso}}$, and of $\mathbf{5_{iso}}$ in comparison to $\mathbf{4_{iso}}$), but further extension of the spacer does not further increase the FIA.

According to the NBO analysis (see Table 3), the formation of the B–N bond to the pyridyl moiety only slightly changes the formal charge at the corresponding boron atom. The high FIA is in part caused by the special structure. To elaborate on this point, the three bond angles (N–B–N, N–B–B and B–B–N) around the three-coordinate boron atom in $\mathbf{5_{iso}}$ are compared with the corresponding angles in $\mathbf{5_{int}}$ with a four-coordinate boron atom (see Supporting Information, Table S1). The angle sum at the boron atom increases upon loss of the triflato group

© 2022 The Authors. Chemistry - A European Journal published by Wiley-VCH GmbH

Table 5. FIA of $\mathbf{1}_{iso}$–$\mathbf{6}_{iso}$ relative to that of $[B_2(hpp)_2]^{2+}$ and relative to the trimethylsilyl cation (TMS^+) calculated with B3LYP + D3/def2-TZVP ($-\Delta H^0$ in kJ mol^{-1}, at 298 K and 1 bar, for the reaction in Scheme 3) with and without inclusion of the solvent effect (COSMO, $\varepsilon_r = 8.93$ for CH_2Cl_2). A positive value means that the FIA is higher than that of $[B_2(hpp)_2]^{2+}$ or TMS^+, respectively.

Compound	FIA vs. $[B_2(hpp)_2]^{2+}$		FIA vs. TMS^+	
	$\varepsilon_r = 1$	$\varepsilon_r = 8.93$	$\varepsilon_r = 1$	$\varepsilon_r = 8.93$
$\mathbf{1}_{iso}$	−47	3	−16	−121
$\mathbf{2}_{iso}$	−25	24	5	−99
$\mathbf{3}_{iso}$	−14	33	16	−91
$\mathbf{4}_{iso}$	−59	−15	−29	−139
$\mathbf{5}_{iso}$	−15	29	16	−95
$\mathbf{6}_{iso}$	−15	27	15	−97

(316.0° for $\mathbf{5}_{int}$, 349.2° for $\mathbf{5}_{iso}$), but the steric constraints imposed by the two bridging hpp substituents prohibit a planar coordination mode of the tri-coordinate boron atom in $\mathbf{5}_{iso}$. Consequently, the Lewis acidity increases.[30] Moreover, according to the NBO analysis for $\mathbf{5}_{iso}$ (Table 3), the three-coordinate B atom [denoted B(P)] carries a high positive charge.

FLP-like chemistry – part b) experimental studies

To test the possible FLP-like chemistry, we used the reaction with *para*-methylbenzaldehyde, since stoichiometric reactions with aldehydes were drawn on frequently to probe the FLP properties.[31–35] Activation of aldehydes can easily be followed via ^{1}H NMR spectroscopy through the loss of the characteristic aldehyde hydrogen signal. Especially, *para*-methylbenzaldehyde turned out to be ideally suited.[32–35] Its bonding to an FLP leads to a characteristic upfield shift of the chemical shift value for the methyl group in the ^{1}H NMR spectra. Furthermore, the process could be followed by the two clearly distinguishable aromatic signals. It turned out that none of the compounds **1**–**5** reacts with an aldehyde. Based on the quantum-chemical calculations, we postulate that kinetic rather than thermodynamic factors prohibit the reaction of compound **5** with *para*-methylbenzaldehyde to the "aldehyde activation product" **7** (Scheme 4a). Indeed, the reaction was calculated to be exergonic with B3LYP + D3/def2-TZVP ($\Delta G = -12$ kJ mol^{-1}). The four-coordinate boron atoms in **1**–**5** only allow substrate binding after B–P bond cleavage (S_N1 mechanism), causing a high reaction barrier. Also, no FLP-like chemistry occurs if potential substrates such as *para*-methylbenzaldehyde (Scheme 4b), carbon dioxide, acetone or *para*-formaldehyde are added to mixtures of the ditriflato-diborane and two equivalents of tri-*tert*-butylphosphane. The corresponding NMR spectra only showed signs of decomposition or unselective reactions. We showed previously that tri-*tert*-butylphosphane does not react with a cationic diborane with bridging hpp substituents, $[B_2H(hpp)_2]^+$, due to steric constraints.[36] The

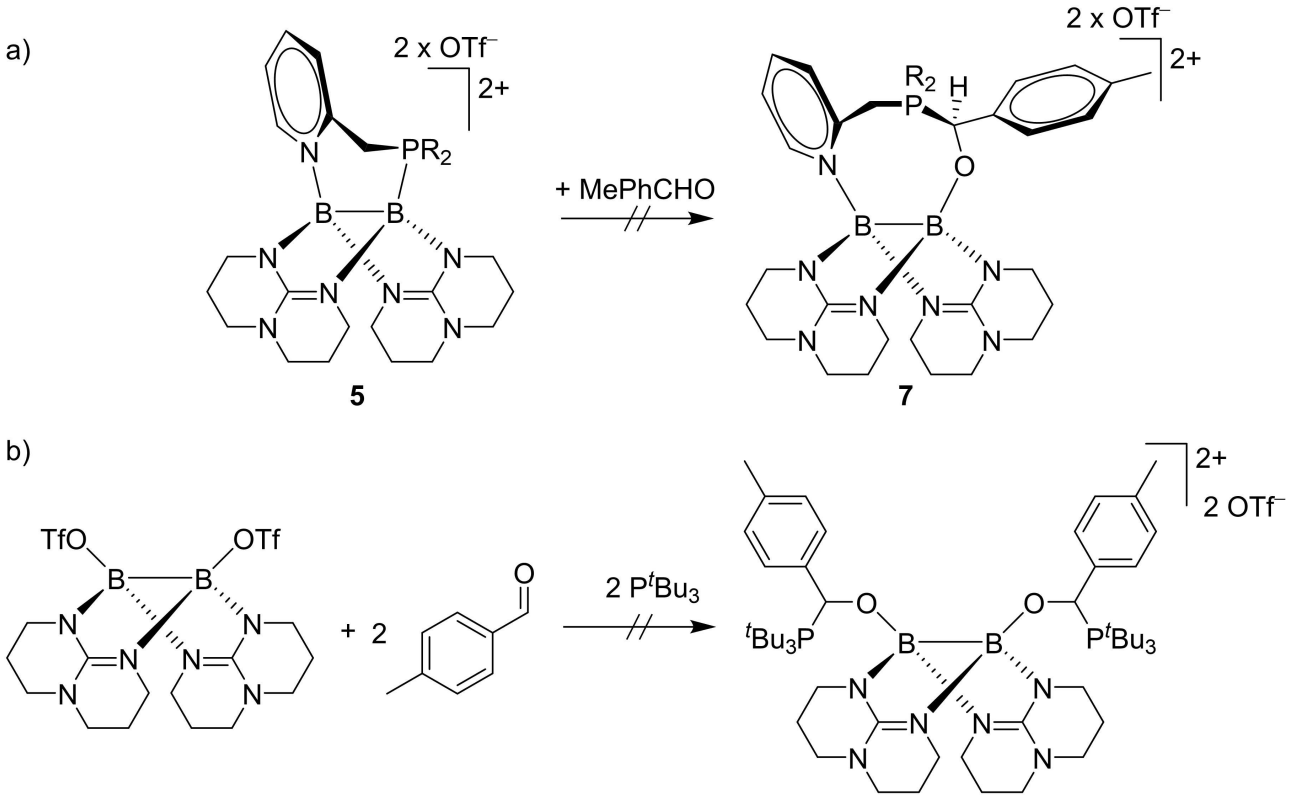

Scheme 4. Unsuccessful attempts to activate *para*-methylbenzaldehyde with a) dicationic diborane **5**, and b) a mixture of the ditriflatodiborane $B_2(hpp)_2(OTf)_2$ and tri-*tert*-butylphosphane.

© 2022 The Authors. Chemistry - A European Journal published by Wiley-VCH GmbH

ditriflato-diborane did not show any signs of reaction with tri-*tert*-butylphosphane either.

Next, we added *para*-methylbenzaldehyde immediately to $\mathbf{5_{int}}$, formed quantitatively in a freshly prepared equimolar mixture of $B_2(hpp)_2(OTf)_2$ and $pyCH_2PtBu_2$. Here, we finally observed an FLP-like chemistry as sketched in Scheme 5, leading to the desired new "aldehyde activation product" **7**. Since our experiments showed that **7** reacts further with aldehyde, we applied a dearth of the aldehyde (ca. 0.44 equiv.). After 1 d, all $pyCH_2PtBu_2$ was consumed, and the aldehyde addition product **7** quantitatively formed. Obviously, aldehyde activation is significantly faster than ring closure to **5**. Eventually, within 5 d the residual molecules of $\mathbf{5_{int}}$ reacted to the inactive ring product **5**, yielding a mixture of ca. 41% of **7** and 59% of **5**. Please note that this yield was entailed by using the dearth of the aldehyde to avoid subsequent reaction of activated aldehyde with free aldehyde. The previously described immediate formation of ca. 10% of **5** upon mixing $B_2(hpp)_2(OTf)_2$ and $pyCH_2PtBu_2$ together, the slowly proceeding ring closing process from $\mathbf{5_{int}}$ to **5**, and the reaction of **7** with excess *para*-methylbenzaldehyde prohibit a higher yield of aldehyde activation product, although the applied aldehyde is quantitatively activated. In the following, the NMR spectra assigned to **7** will be discussed in detail.

Figures 8 and 9 show representative NMR spectra. Although the reaction with the aldehyde is completed in 1 d, we generally waited 5 d to ensure full conversion of $\mathbf{5_{int}}$, either to **7** or to **5**. First, the aldehyde hydrogen signal of *para*-methylbenzaldehyde at $\delta = 9.94$ ppm is absent in the ^{1}H NMR of the reaction mixture, indicating complete aldehyde conversion. The aromatic region of the ^{1}H NMR spectra indeed showed the sole presence of two distinct molecules (Figure 7a). The signals at $\delta = 8.73$ and 8.28 ppm and some signals in the multiplet at $\delta =$ 7.98 ppm belong to the inactive ring product **5**. According to COSY NMR measurements, the signals at $\delta = 8.68$, 8.47 and 8.24 ppm and some signals in the multiplet at $\delta = 7.98$ ppm belong to a second species with a pyridyl entity, identified as the activation product **7**. Furthermore, the signals at $\delta = 7.54$ and 7.20 ppm, with twice the intensity of the antecedent signals, are assigned to **7**. A singlet at $\delta = 5.67$ ppm is due to a hydrogen atom without neighboring hydrogens in the structure assigned to **7** (Figure 7b). The corresponding carbon nucleus gives rise to a doublet in the $^{13}C\{^1H\}$ NMR spectrum at $\delta =$ 76.3 ppm, verifying its bonding to a P nucleus, in line with the Lewis structure of **7**. Furthermore, two signals at $\delta = 4.80$ and 4.62 ppm indicate the presence of two diastereotopic hydrogen atoms bound to the same C atom according to HSQC measurements (see Supporting Information, Figure S16). This is similar to the results obtained for compound **3**; for its seven-membered ring structure no racemization of the ring structure is observed, leading to distinct signals in the ^{1}H NMR spectrum for the hydrogens in the ethylene bridge as well as for the hydrogens in the different phenyl entities. Since **7** exhibits an eight-membered ring, a similar effect is expected.

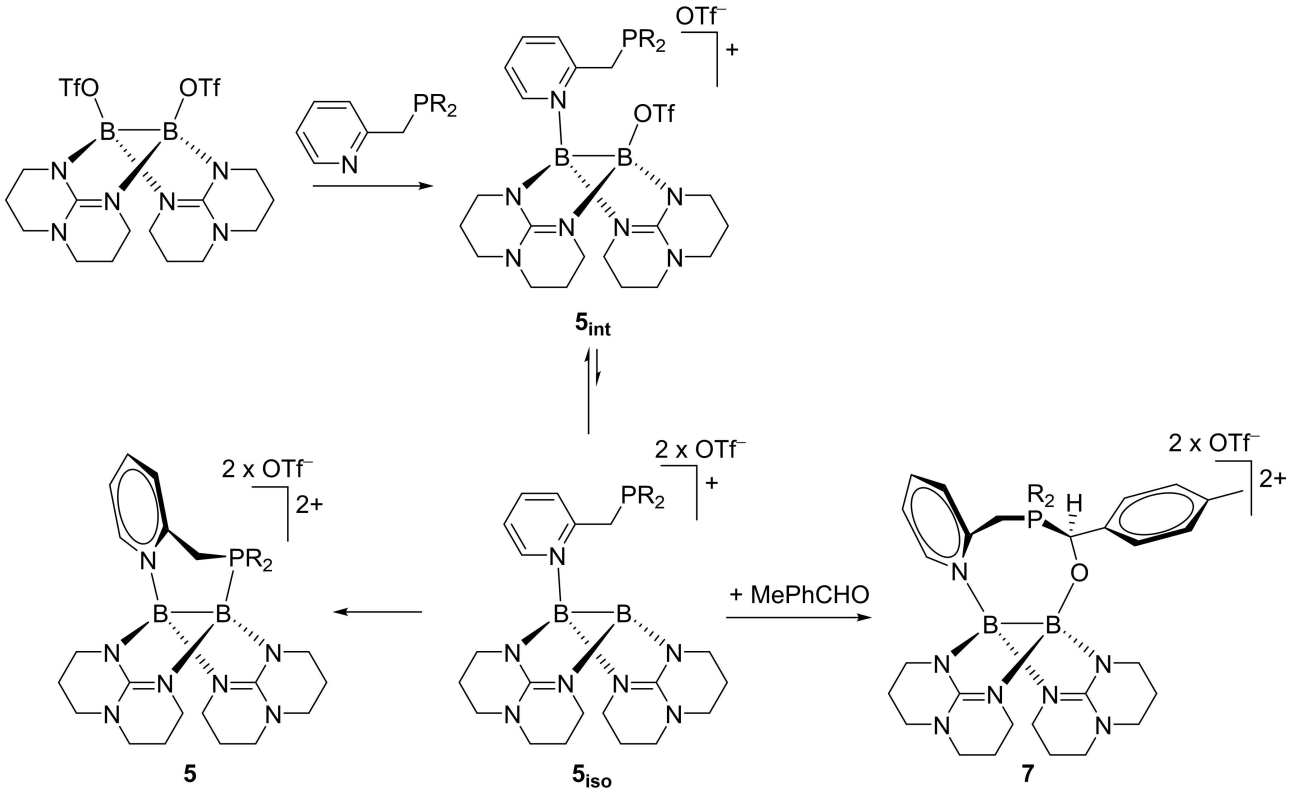

Scheme 5. Possible pathway of the reaction between the ditriflato-diborane $B_2(hpp)_2(OTf)_2$ and $pyCH_2PtBu_2$ to give first $\mathbf{5_{int}}$ ("FLP resting state"), from which $\mathbf{5_{iso}}$ is generated in a triflate elimination equilibrium. $\mathbf{5_{int}}$ is either converted through $\mathbf{5_{iso}}$ in a very slow reaction to **5**, or activates the aldehyde (*para*-methylbenzaldehyde) to give **7**. R = *t*Bu.

© 2022 The Authors. Chemistry - A European Journal published by Wiley-VCH GmbH

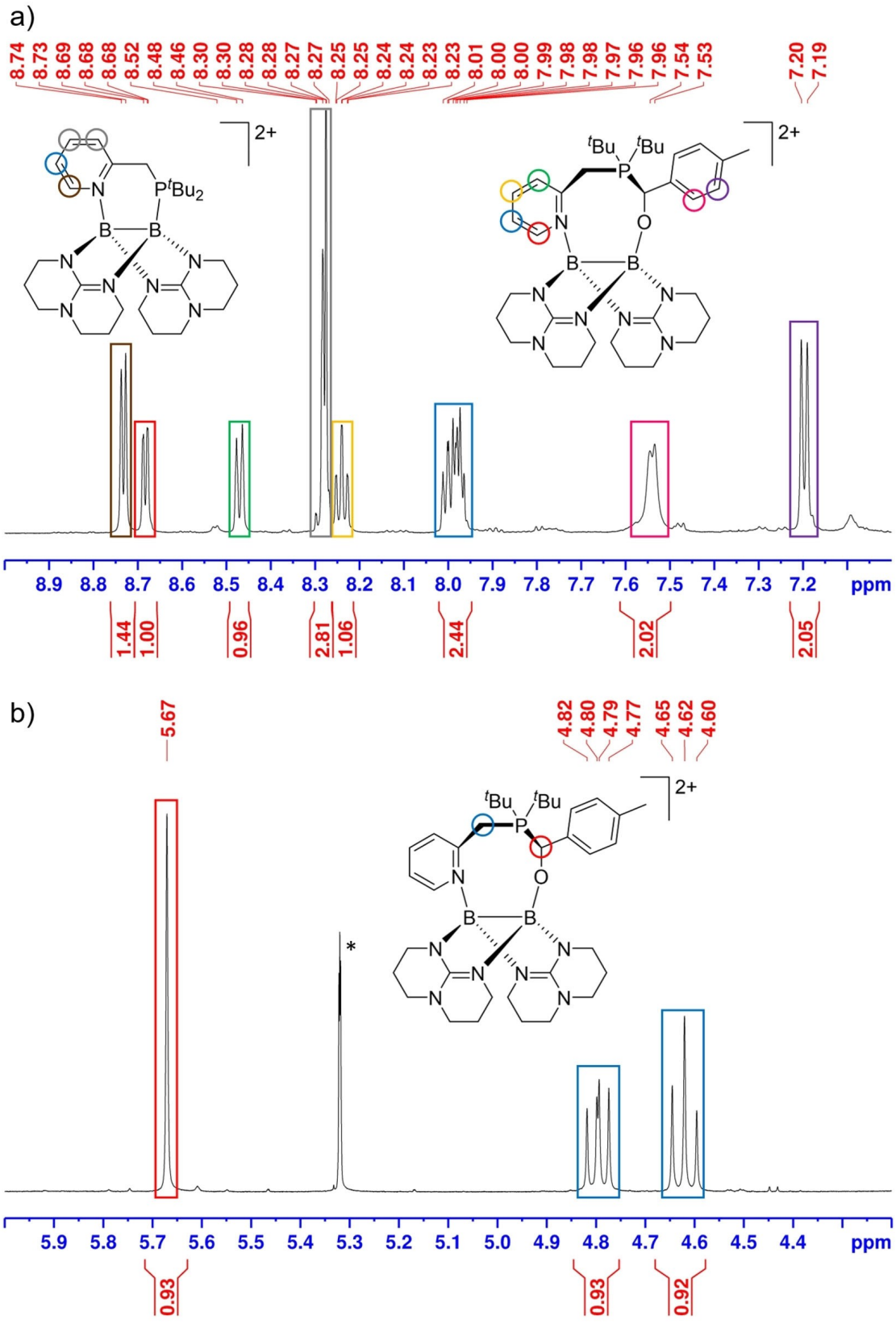

Figure 7. Sections a) between $\delta = 9.0$ and 7.0 ppm typical for aromatic protons, and b) between $\delta = 6.0$ and 4.2 ppm of the ^{1}H NMR spectrum (600.18 MHz, CD_2Cl_2), recorded after 5 d for a mixture of the ditriflato-diborane and $PyCH_2PtBu_2$ to which *para*-methylbenzaldehyde was added. The spectra indicate the sole presence of molecules **7** and **5**. The solvent signal is highlighted by an asterisk.

© 2022 The Authors. Chemistry - A European Journal published by Wiley-VCH GmbH

Two signals appear in the ^{31}P NMR spectrum (Figure 8a). The signal at $\delta = 23.62$ ppm is due to the ring product **5**. The second signal at $\delta = 57.39$ ppm shows fine coupling, indicating the absence of a bond to a B atom which would, as in **5**, broaden the signal and suppress the observation of a coupling pattern. Therefore, this second signal is assigned to the activation product **7**. The ^{11}B NMR spectrum shows, besides the signals at $\delta = 3.50$ and -4.44 ppm from **5**, a signal at higher shift values assigned to **7** (Figure 8b, black curve). A second ^{11}B NMR signal from the unsymmetric activation product **7** emerges after subtraction of the ^{11}B NMR spectrum of **5** (Figure 8b, red curve). Thus, signals at $\delta = 5.92$ and 3.34 ppm belong to **7** (Figure 8b, green curve).

Furthermore, all signals due to the 31 distinguishable carbon atoms in **7** are observed in the $^{13}C\{^1H\}$ NMR spectrum (see Supporting Information, Figures S17 and S18). Thus, the spectra clearly confirm reaction to **7**.

Excess of *para*-methylbenzaldehyde led to a new singlet signal at $\delta = 5.75$ ppm in the ^{1}H NMR spectrum (see Supporting Information, Figure S19). The corresponding $^{13}C\{^1H\}$ NMR signal at $\delta = 85.8$ ppm did not show any CP coupling, indicating loss of the C–P bond. Moreover, a new ^{31}P NMR signal emerged at $\delta = 41.94$ ppm, and a further minor doublet signal ($^1J_{PH} = 463$ Hz) grew in at $\delta = 44.90$ ppm (see Supporting Information, Figure S19), indicating the formation of a P–H bond. Unfortunately, so far the resulting product could neither be isolated nor identified.

Interestingly, only one isomer is detected for the activation product **7**. On the other hand, two distinct diastereomers are possible, depending on the pre-orientation of $\mathbf{5_{int}}$ and the mode of attack (*re* or *si* face) at the *para*-methylbenzaldehyde (Figure 9a). Quantum-chemical calculations (B3LYP + D3/def2-TZVP) indicate that isomer **7A** is energetically favored by $\Delta G = -17$ kJ mol^{-1}. Furthermore, compared to **5** and *para*-methylbenzaldehyde, isomer **7A** is exergonic ($\Delta G = -12$ kJ mol^{-1}), but isomer **7B** endergonic ($\Delta G = +5$ kJ mol^{-1}), explaining the exclusive formation of isomer **7A**.

To obtain additional information, we calculated the NMR shifts for both isomers of **7**. The former aldehyde carbon is calculated to show at $\delta = 86.5$ ppm for isomer **7A** and $\delta = 83.1$ ppm for isomer **7B** in the $^{13}C\{^1H\}$ spectra, whereas the experimental $^{13}C\{^1H\}$ spectrum shows a signal at $\delta = 76.3$ ppm in CD_2Cl_2 solution. Although the calculated values deviate from the experimental ones, both calculation and experiment found a signal in an area quite unusual for ^{13}C signals. The calculations indicate that the signals from the two isomers should differ in their chemical shifts (see Supporting Information, Table S2). Therefore, they are consistent with the formation of only one isomer, being the thermodynamically favored compound **7A**.

Proposal for a new type of FLP-like chemistry

The results presented in the last section clearly show that $\mathbf{5_{int}}$ displays FLP-like chemistry. An aldehyde is bound by the combined Lewis acidic and Lewis basic properties of $\mathbf{5_{iso}}$, formed in a triflate elimination equilibrium from $\mathbf{5_{int}}$. The Lewis acidic site is not blocked by the triflate substituent, since triflate is readily eliminated. The results also show that binding of the pyridyl moiety is crucial for the FLP system. It enables the formation of an intramolecular FLP system, placing the phosphorus Lewis base close to the boron Lewis acid, and simultaneously oppresses side reactions. The application of the new compound in FLP-like chemistry requires the presence of a hemilabile (triflato) substituent, that could easily be eliminated. The formation of the B-P bond has to be prohibited, since substrate activation by the four-coordinate boron atom is kinetically disfavored (Scheme 5). The undesired B–P ring closure reaction is hampered by the steric constraints imposed by the alkyl spacer and the two *tert*-butyl substituents on the P atom, in combination with the slow triflate elimination equilibrium. The triflato substituent acts as a "protecting group", that prohibits undesired reaction channels.

Based on these results, we propose a new type of FLP-like reactivity, as sketched in Scheme 6, relying for the first time on the Lewis acidity of dicationic diboranes.

The peculiarities of this new type could be summarized as follows.

1) A molecule with two Lewis basic sites B1 and B2 (a pyridyl and a phosphino group) is used, one accomplishing bonding to the diboron compound (B1, the pyridyl group) and the other being responsible for substrate activation (B2, the phosphino group). Here, the pyridyl group turned out to be the ideal choice for B1; it rapidly forms a bond to one of the boron atoms, and leads to a high positive charge on the diboron unit, thereby increasing its Lewis acidity.
2) The Lewis-acidic, four-coordinate boron atom in $\mathbf{5_{int}}$ used for the FLP-like chemistry is bound to a hemilabile substituent (triflate), creating an "FLP resting state" from which the strong boron Lewis acid is generated in equilibrium. Due to the four-coordinate boron atom, substitution reactions must follow an S_N1 mechanism. The readily eliminated hemilabile substituent in the "FLP resting state" stabilizes the diboron reagent, protects the Lewis acidic site from attack by other nucleophiles, and increases the selectivity.
3) Steric constraints, imposed by the alkyl spacer between the pyridyl and a phosphino group with sterically-demanding substituents, lead to a significant barrier for the undesired B–P ring closure reaction.
4) The Lewis acidity of the boron atom after triflate elimination is further increased by its non-planarity, imposed by the bridging hpp substituents.

The Lewis-basic sites B1 and B2 and the linker between them are valuable parameters to tune the reactivity. A pyridyl group is an optimal choice for B1, as it binds very fast to the B atom, endues the diboron unit with a positive charge that increases its Lewis acidity, and places the B2 base close to the boron atom.

Conclusion

Starting with the ditriflato-diborane $B_2(hpp)_2(OTf)_2$ with two highly-electron donating bridging hpp substituents (hpp =

© 2022 The Authors. Chemistry - A European Journal published by Wiley-VCH GmbH

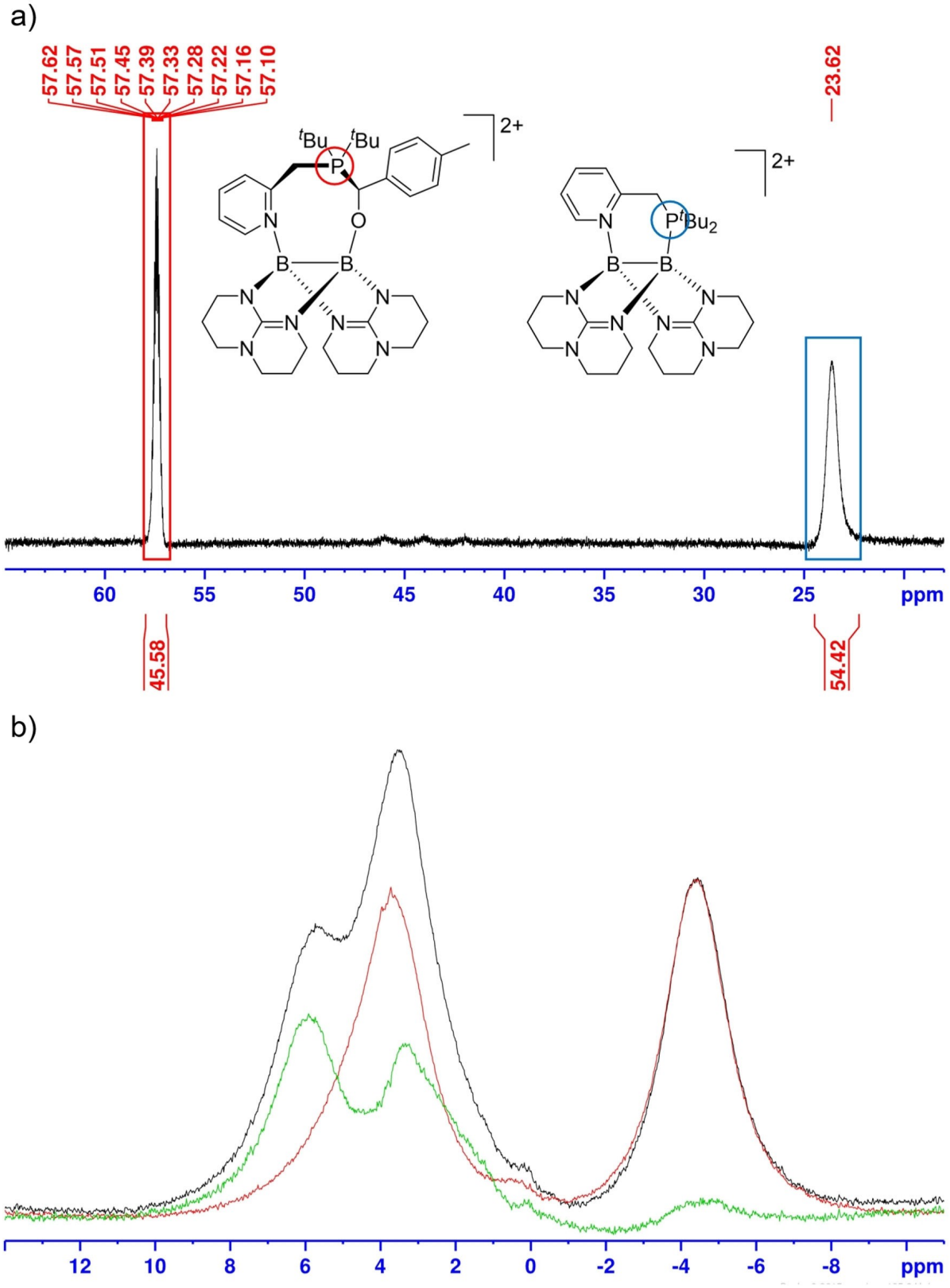

Figure 8. a) ^{31}P NMR spectrum (242.96 MHz, CD_2Cl_2), recorded for a mixture of $B_2(hpp)_2(OTf)_2$ and $PyCH_2P^tBu_2$, to which *para*-methylbenzaldehyde was added, showing signals due to **5** and **7**. b) ^{11}B NMR spectrum (192.56 MHz, CD_2Cl_2) of the same reaction mixture taken after 5 d (black). Upon subtraction of the signals from **5** at $\delta = 3.50$ and -4.44 ppm (red), the signals at $\delta = 5.92$ and 3.34 ppm due to **7** emerge (green).

© 2022 The Authors. Chemistry - A European Journal published by Wiley-VCH GmbH

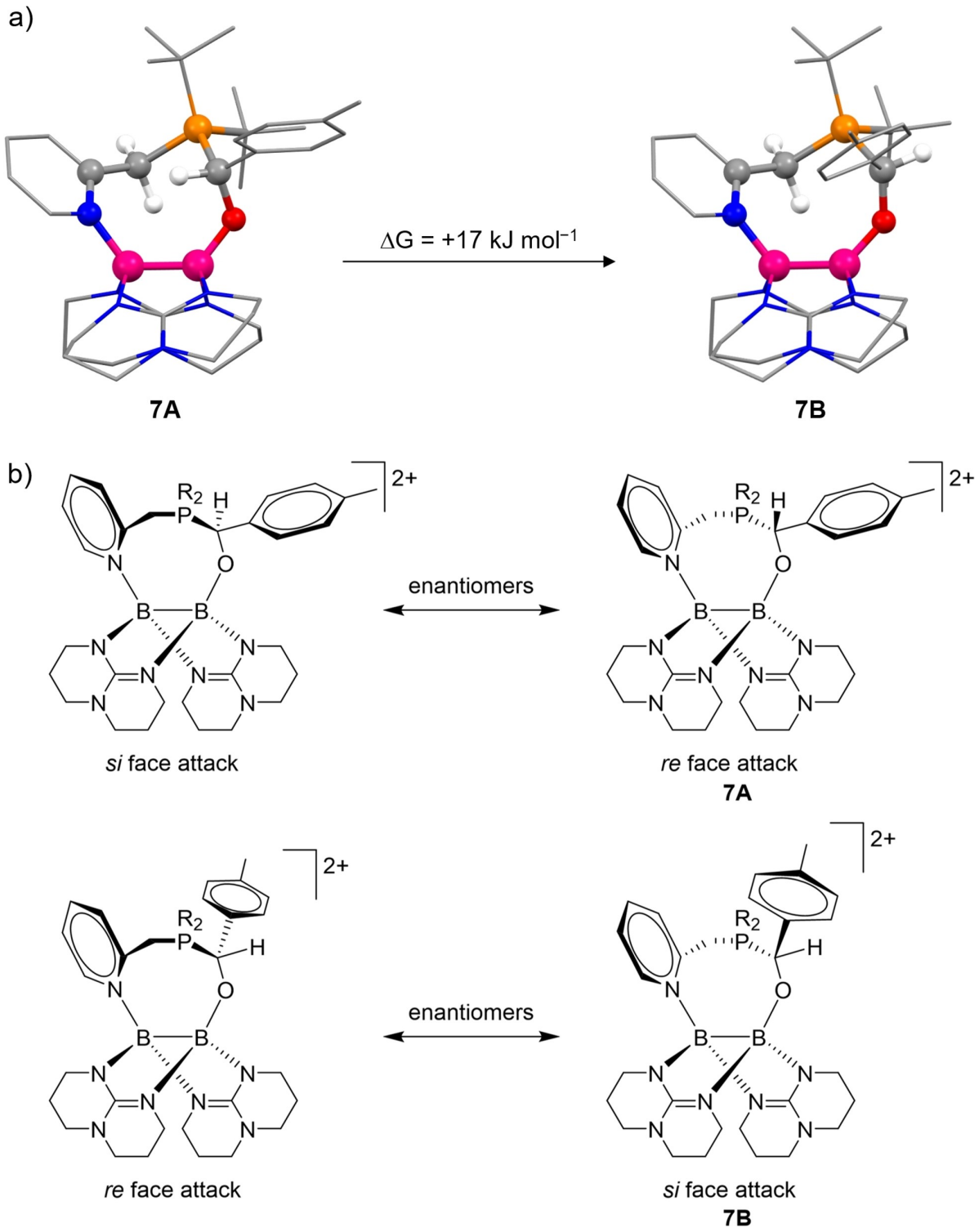

Figure 9. a) Illustration of the calculated structures for isomers **7 A** and **7B** (B3LYP + D3/def2-TZVP), resulting from activation of *para*-methyl-benzene by $\mathbf{5}_{int}$ in a *re* (**7 A**) or *si* face attack (**7B**). b) Structural influence of the different pre-orientations of $\mathbf{5}_{int}$ on the resulting activation product. The different enantiomers of the adduct require opposite *re*/*si* face attack to form corresponding product enantiomers. Thus, *re* face or *si* face attack is not a criterion to discriminate between the two isomers.

1,3,4,6,7,8-hexahydro-2*H*-pyrimido[1,2-α]pyrimidinate) and two tetra-coordinate boron atoms, several new, stable, unsymmetric dicationic diboranes were synthesized by reaction with phosphino-pyridine molecules that provide two Lewis basic sites to bind to the two boron atoms of the diboron unit. In S_N1 reactions, the triflato groups are successively substituted. First,

© 2022 The Authors. Chemistry - A European Journal published by Wiley-VCH GmbH

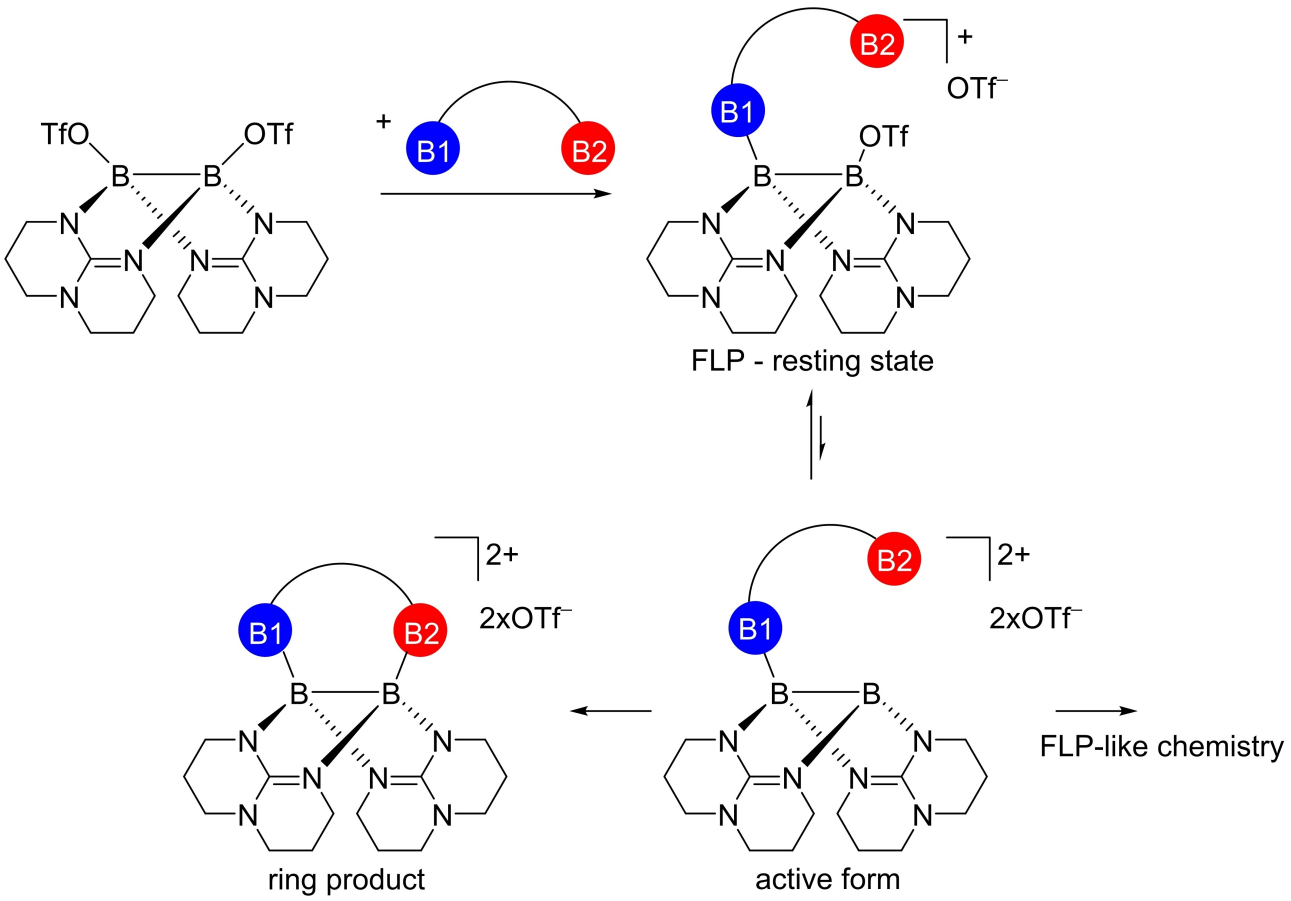

Scheme 6. Draft of a new type of FLP reactivity using for the first time dicationic diboranes as Lewis acid component. The active intramolecular Lewis pair is generated in an equilibrium from a "FLP resting state". Frustration arises from steric constraints in combination with an elimination/addition equilibrium of a triflate, that hampers the formation of a bond between B2 and the boron atom prior to substrate activation.

the pyridine N atom is bound in a fast reaction to one of the boron atoms, creating a monocationic diborane in which the positive charge is localized on the diboron unit. Then, a second S_N1 reaction leads to elimination of the second triflate and formation of the B–P bond. The properties of the resulting new dicationic diboranes were evaluated, and the experimental analysis complemented by quantum-chemical calculations.

Formation of the dicationic diboranes generally proceeds fast, the only exception being the reaction with 2-((di-*tert*-butylphosphino)methyl)pyridine. In this case, substitution of the first triflate by the phosphino-pyridine is fast, resulting in the intermediate $\mathbf{5}_{int}$, in which only the pyridine N atom is bound to the diboron unit. The substitution of the second triflate and formation of the B–P bond to give **5** is slow, requiring 3 d for completion. The intermediate $\mathbf{5}_{int}$ represents a type of "FLP resting state", that could be used for molecule activation. As example, we reacted the intermediate with *para*-methylbenzaldehyde to give quantitatively the activation product **7**. Based on the results of this work, we suggest a new type of FLP-like reactivity as outlined in Scheme 6, resorting for the first time to dicationic diboranes as Lewis acids. The formation of the bond between B1 and the diborane creates a stable "FLP resting state", from which the active form is generated in an elimination equilibrium. The positive charge imposed by the neutral B1 base and the non-planarity of the boron acid in the active form further boost the Lewis acidity of the boron atom.

In the future we want to extend our work in this direction with the aim to establish dicationic diboranes as Lewis acidic components in FLP-like chemistry. In contrast to monoboranes, the diborane is capable to pre-orient the Lewis-base by binding to a second Lewis-basic site of the same molecule. In future work, we also try to combine FLP-like substrate activation with electron-transfer from the diboron unit to the substrate.

Acknowledgements

The authors gratefully acknowledge financial support by the German research foundation (DFG). The authors acknowledge support by the state of Baden-Württemberg through bwHPC and the German Research Foundation (DFG) through grant no INST 40/575-1 FUGG (JUSTUS 2 cluster). Open Access funding enabled and organized by Projekt DEAL.

© 2022 The Authors. Chemistry - A European Journal published by Wiley-VCH GmbH

Conflict of Interest

The authors declare no conflict of interest.

Data Availability Statement

The data that support the findings of this study are available in the supplementary material of this article.

Keywords: boron · diborane · dication · frustrated Lewis pair · Lewis acid

[1] I. B. Sivaev, V. I. Bregadze, *Coord. Chem. Rev.* **2014**, *270–271*, 75–88.
[2] J. R. Lawson, R. L. Melen, *Inorg. Chem.* **2017**, *56*, 8627–8643.
[3] G. C. Welch, R. R. S. Juan, J. D. Masuda, D. W. Stephan, *Science* **2006**, *314*, 1124–1126.
[4] D. W. Stephan, *Dalton Trans.* **2009**, 3129–3136.
[5] D. W. Stephan, G. Erker, *Angew. Chem.* **2010**, *122*, 50–81; *Angew. Chem. Int. Ed.* **2010**, *49*, 46–76.
[6] G. Erker, *C. R. Chim.* **2011**, *14*, 831–841.
[7] T. Wiegand, H. Eckert, O. Ekkert, R. Fröhlich, G. Kehr, G. Erker, S. Grimme, *J. Am. Chem. Soc.* **2012**, *134*, 4236–4249.
[8] D. W. Stephan, *Org. Biomol. Chem.* **2012**, *10*, 5740–5746.
[9] a) D. W. Stephan, *Top. Curr. Chem.* **2013**, *332*, 1–44; b) G. Kehr, S. Schwendemann, G. Erker, *Top. Curr. Chem.* **2013**, *332*, 45–84; c) D. W. Stephan, G. Erker, *Top. Curr. Chem.* **2013**, *332*, 85–110.
[10] D. W. Stephan, G. Erker, *Angew. Chem.* **2015**, *127*, 6498–6541; *Angew. Chem. Int. Ed.* **2015**, *54*, 6400–6441.
[11] D. W. Stephan, *Acc. Chem. Res.* **2015**, *48*, 306–316.
[12] P. Kölle, H. Nöth, *Chem. Rev.* **1985**, *85*, 399–418.
[13] W. E. Piers, S. C. Bourke, K. D. Conroy, *Angew. Chem.* **2005**, *117*, 5142–5163; *Angew. Chem. Int. Ed.* **2005**, *44*, 5016–5036.
[14] T. S. De Vries, A. Prokofjevs, E. Vedejs, *Chem. Rev.* **2012**, *112*, 4246–4282.
[15] P. Eisenberger, C. M. Crudden, *Dalton Trans.* **2017**, *46*, 4874–4887.
[16] D. Franz, S. Inoue, *Chem. Eur. J.* **2019**, *25*, 2898–2926.
[17] H.-J. Himmel, *Angew. Chem.* **2019**, *131*, 11724–11742; *Angew. Chem. Int. Ed.* **2019**, *58*, 11600–11617.
[18] A. Widera, E. Filbeck, H.-J. Himmel, *Eur. J. Inorg. Chem.* **2020**, 3017–3029.
[19] R. Dinda, O. Ciobanu, H. Wadepohl, O. Hübner, R. Acharyya, H.-J. Himmel, *Angew. Chem.* **2007**, 119, 9270–9273; *Angew. Chem. Int. Ed.* **2007**, *46*, 9110–9113.
[20] L. Kong, W. Lu, Y. Li, R. Ganguly, R. Kinjo, *J. Am. Chem. Soc.* **2016**, *138*, 8623–8629.
[21] A. Widera, D. Vogler, H. Wadepohl, E. Kaifer, H.-J. Himmel, *Angew. Chem.* **2018**, *130*, 11627–11630; *Angew. Chem. Int. Ed.* **2018**, *57*, 11456–11459.
[22] M. Möhlen, B. Neumüller, N. Faza, C. Müller, W. Massa, K. Dehnicke, *Z. Anorg. Allg. Chem.* **1997**, *623*, 1567–1576.
[23] N. Arnold, H. Braunschweig, R. D. Dewhurst, F. Hupp, K. Radacki, A. Trumpp, *Chem. Eur. J.* **2016**, *22*, 13927–13934.
[24] D. Franz, T. Szilvasi, A. Pöthig, F. Dieser, S. Inoue, *Chem. Eur. J.* **2018**, *24*, 4283–4288.
[25] F. Schön, L. Greb, E. Kaifer, H.-J. Himmel, *Angew. Chem.* **2020**, *132*, 9212–9218; *Angew. Chem. Int. Ed.* **2020**, *59*, 9127–9133.
[26] A. Widera, H. Wadepohl, H.-J. Himmel, *Angew. Chem.* **2019**, *131*, 5957–5961; *Angew. Chem. Int. Ed.* **2019**, *58*, 5897–5901.
[27] J. Lam, K. M. Szkop, E. Mosaferi, D. W. Stephan, *Chem. Soc. Rev.* **2019**, *48*, 3592–3612.
[28] Deposition Numbers 2117116 (for **1**$(OTf)_2$), 2117117 (for **2**$(OTf)_2$), 2117115 (for **3**$(OTf)_2$), 2117114 (for **4**$(OTf)_2$) contain the supplementary crystallographic data for this paper. These data are provided free of charge by the joint Cambridge Crystallographic Data Centre and Fachinformationszentrum Karlsruhe Access Structures service.
[29] J. Horn, A. Widera, S. Litters, E. Kaifer, H.-J. Himmel, *Dalton Trans.* **2018**, *47*, 2009–2017.
[30] A. Chardon, A. Osi, D. Mahaut, A. B. Saida, G. Berionni, *Synlett* **2020**, *31*, 1639–1648.
[31] A. Stute, G. Kehr, C. G. Daniliuc, R. Fröhlich, G. Erker, *Dalton Trans.* **2013**, *42*, 4487–4499.
[32] D. Hartmann, S. Braner, L. Greb, *Chem. Commun.* **2021**, *57*, 8572–8575.
[33] E. Anders, F. Markus, H. Meske, J. Tropsch, G. Maas, *Chem. Ber.* **1987**, *120*, 735–745.
[34] E. Anders, K. Hertlein, H. Meske, *Synthesis* **1990**, *4*, 323–326.
[35] E. Anders, K. Hertlein, A. Stankowiak, E. Irmer, *Synthesis* **1992**, *6*, 577–582.
[36] S. Litters, M. Ganschow, E. Kaifer, H.-J. Himmel, *Eur. J. Inorg. Chem.* **2015**, 5188–5195.

Manuscript received: November 8, 2021
Accepted manuscript online: January 21, 2022
Version of record online: February 10, 2022

© 2022 The Authors. Chemistry - A European Journal published by Wiley-VCH GmbH